Perturbations of Dipole Decay Dynamics Induced by Plasmonic Nano-antennas – A Study within the Discrete Dipole Approximation

Invited Review Article

Stefania D'Agostino[1,2]*, Fabio Della Sala[1,3] and Lucio Claudio Andreani[2]

1 Center for Biomolecular Nanotechnologies @UNILE, Istituto Italiano di Tecnologia (IIT), Arnesano, Italy
2 Physics Department, University of Pavia, Pavia, Italy
3 Istituto Nanoscienze-CNR, Euromediterranean Center for Nanomaterial Modelling and Technology (ECMT), Lecce, Italy
* Corresponding author(s) E-mail: stefania.dagostino@iit.it

Abstract

We report a discrete dipole approximation approach to analyse the perturbations induced by silver nano-particles on the decay dynamics of a point-like emitter placed in their proximity. Due to the excitation of localized surface plasmons, metallic nano-particles behave like optical antennas and are able to convert localized fields into free-propagating optical radiation, and vice versa. Field localization and enhancement induce strong changes on the decay dynamics of dipoles located in the perturbed electromagnetic environment, and these can be faithfully quantified within the framework of classical electromagnetism in terms of total, radiative and non-radiative decay rates. The method is tested on benchmark cases, i.e., nano-spheres and nano-shells, and it is then applied to analytically-unsolvable shapes such as sharp nano-cones and oxide-covered small nano-antennas. Numerical results reveal 10^5-order enhancements in the total decay rate of the dipole when located very near to the sharp tip, both with and without a thin Ag_2O layer. Moreover, the counter-intuitive behaviour of the cone response in relation to the distance between the metal and the source of the radiation is discussed. Applications span from strong coupling studies to time-resolved fluorescence spectroscopy.

Keywords Discrete Dipole Approximation, Optical Antennas, Localized Plasmons, Dipole Decay Dynamics

1. Introduction

Since the pioneering work of Purcell in 1946 [1], it has been widely known in the field of fluorescence spectroscopy that the rate of the emission process can be modified by placing a quantum emitter (QE), such as an atom or a molecule, in a structured polarizable environment [2 - 5]. Usually, the interaction between the emitter and its local optical environment is such that only the spontaneous emission rate is perturbed, while the emission frequency remains unaltered. In this regime of light-matter interaction, called a *weak coupling regime*, a fundamental goal of the research has been to quantify the changes induced by the surround-

ing medium on the emitter decay dynamics, while at the same time clarifying the balance between the radiative and the nonradiative decay channels [6 - 8].

In recent years, the plasmonics community has looked with increasing interest at the possibility of handling the modification of spontaneous emissions through the conscious and controlled use of localized and delocalized surface plasmons, this favouring the growth of *radiative decay-rate engineering* (RDE) [9] which has become a central issue in nano-photonics. Metallic nano-structures and nano-patterned surfaces provide, in fact, a unique way to increase the radiative decay rate of fluorophores, and it has been shown that unusual effects on fluorophores, such as increasing or decreasing the rates of radiative decay or resonance energy transfer (RET), can be achieved [10]. Moreover, due to both the extreme tunability of the plasmonic response and the near field enhancement in metallic nano-particle assemblies or geometries, plasmonics offers unprecedented opportunities for controlling light at the nano-scale. Thus, it allows us to neatly engineer the coupling between the electronic excitations of the emitter and the collective motion of the metallic electrons in the plasmons.

This important, plasmon-mediated engineering now becomes possible thanks to the extremely precise control that we have over the plasmonic modes supported by metallic nano-structures. This control derives either from the consolidated understanding of the relationship between the details of the nano-structure and the nature of the associated plasmon modes, or from the last experimental developments of powerful and impressive nano-fabrication and characterization techniques. The development of nano-optics techniques has, thus, greatly contributed to affirming the importance of exploiting plasmonic nano-antennas, like metallic nano-particles or nano-tips, and to modifying the excited-state lifetime [11], the fluorescence intensity [11 - 19], and the radiation distribution [17, 20] of isolated emitters. Due to the highly confined electromagnetic resonances following from the response of free electrons [12], metallic nano-particles or nano-structures are in fact able to strongly perturb the electromagnetic fields in their surroundings and to modify both the excitation and the emission rates of proximate fluorophores, chromophores and QDs [21].

Despite these experimental examples, the problem of the electromagnetic coupling between a plasmonic object and a source of radiation located in its proximity continues to raise numerous open questions in molecular plasmonics, especially for complex nano-particle shapes that do not lend themselves to an analytical treatment.

Theoretically, the investigation of electrodynamic coupling between molecules and metal nano-particles can be worked out with different levels of approximation according to the description used for the counterparts, and different options can be found in the literature. According to a widely-used approach, the molecule is considered as a classical oscillating point dipole, and the metal nano-particle as a continuous body characterized by its own frequency-dependent dielectric function [13].

In the regime of very narrow junctions and sub-nanometre metal-molecule distances, other interactions become important, and chemical effects must also be included in the treatment [22 - 24]. These primarily comprise the nonlocal screening or the finite spatial profile of the plasmon-induced screening charge, and the spill-out or tunnelling of electrons outside the nano-particle surfaces [25, 26]. Treating these interactions is sometimes mandatory for a complete understanding of some molecular plasmonics phenomena, and as such a more sophisticated method has been developed to study the coupling. It consists of exploiting the continuous body description of the metal and of treating the molecule atomistically by standard electronic structure techniques, such as time-dependent Hartree-Fock (TDHF) and time-dependent density functional theory (TD-DFT), which include the electromagnetic interaction in the molecular Hamiltonian [27, 28], and by performing a fully quantum mechanical analysis of both the counterparts (i.e., the QE and the metal) [25, 26].

Here, a classical electrodynamics description of a metal-emitter system is adopted to quantitatively study the perturbations induced by nano-particles to the spontaneous decay rate of a single emitter taken to be point-like, in a regime of weak coupling in which a macroscopic description of metal is assumed to be valid [29].

A discrete dipole approximation (DDA) [30, 31] approach is presented as a useful and accurate tool to investigate coupling problems involving geometries that are not analytically solvable and for which more accurate approaches (partially or fully *ab initio*) could prove prohibitive. The idea at the basis of the analysis involves accurately describing the nano-particle shape to acquire a faithful description of the optical response of the metallic component on the emitter, this being necessary to quantify the perturbations induced on the decay dynamics of the dipole. A vast literature on DDA exists - it mostly concerns the solution of the Maxwell problem for metallic structures excited by plane waves or radiations coming from infinitely-distant sources. In studying plasmonic antennas' behaviour, generally, we have to deal with strongly variable electromagnetic fields emitted by dyes or QDs placed near the metal nano-structure. Since, for a first approximation, the finite size of such kinds of emitters can be ignored (their dimensions being much smaller than electromagnetic wavelengths in the VIS-NIR range), and these can be considered as point-like radiating dipoles, a very attractive possibility would be to extend the numerical methods (e.g., DDA, the *boundary elements method*, the *finite element method*, etc.) to include incident fields assuming the form of dipolar fields.

The focus of this review is to summarize the recent developments in this field regarding the DDA method [32 - 34] and to illustrate the working principles and the potential of a new implementation of DDA, including incident fields generated by local point-like sources [35]. Despite the vast literature in the field [8, 36 - 53], to the best of our knowledge, a crucial issue remains in demonstrating the reliability of a general purpose numerical approach for calculating the total, radiative and non-radiative decay rates of a metal-emitter system.

In this paper, a preliminary check performed in two different cases for which an analytical solution exists (spheres and nano-shells) shows excellent agreement between exact and numerical results for the decay rate modification, thus placing the method on a firm ground. The analysis reported here aims to shed light on the perturbations on the dipole decay rates induced by 10 nm-sized Ag nano-particles. In particular, the differences between spherically-shaped nano-particles and conically-shaped ones are underlined in the dependence of the antennas' response on the dipole distance and orientation: numerical results assess the capability of a sharp Ag nano-cone to strongly modify the lifetime of an emitter with high sensitivity on the dipole distance and orientation with respect to the tip. Numerical results reveal 10^5-order enhancements in the total decay rate of the dipole when located very near to the sharp tip. This is of huge importance, as an example, for the onset of strong coupling interactions [34, 54].

In addition, we present novel results on oxidated nano-particles. We included a thin Ag_2O layer covering the nano-particles with the aim of shedding light on the effects of oxidation on the optical behaviour of this kind of Ag nano-particle. The appearance of a few nanometres of native oxide represents, in fact, a real problem in plasmonics applications for metals, e.g., silver and aluminium, and can be revealed by SEM images or x-ray diffraction analysis after a few minutes of exposure to air [55, 56]. We found that the oxide layer produces a red-shift of the major resonances and increased field localization inside the metal.

The remaining part of the paper is organized as follows. In Sec. II, we summarize the theoretical and computational method by underlining the relationship existing among the normalized decay rates (radiative, non-radiative and total). The reliability of the method is then shown and discussed in Sec. III by comparing the DDA decay rates for Ag nano-spheres and nano-shells with the exact electrodynamic results that are well-known for these geometries. In Sec. IV, we then calculate the dipole total decay rate modifications in the proximity of variously-shaped small Ag nano-particles (spheres, nano-shells and cones) with and without a thin silver oxide layer covering the nano-particle and study the dependence of them on the emitter distance and orientation. In Sec. V, conclusions are drawn.

2. Dipole Decay Rates: Theory and Method

The perturbations on the dipole decay dynamics induced by the plasmonic background are analysed here in the framework of the DDA [30, 31, 57] full-wave simulation method, which describes the scatterer as an array of polarizable dipolar elements organized on a regular cubic grid. The polarization of each element is the result of the interaction with the local electromagnetic field produced by all the other elements plus the external field. This method yields solutions for the electromagnetic field in response to an incident electric field in the frequency domain, including retardation effects. By simply fixing the dipole position in the space, we take care of the antenna response and of the perturbations induced by it on the local field at the dipole position in a rigorous way.

We assume a point-like dipole $\tilde{\mathbf{p}}_0$ (this, and other complex quantities throughout this paper, will be indicated with the grapheme placed at $\mathbf{r}_0$ and emitting electromagnetic radiation with a frequency ω near a metallic nano-particle *in a vacuum*. This nano-particle reflects and/or scatters-back radiation by generating a response electric field $\tilde{\mathbf{E}}_{scat}$ given by [57]

$$\tilde{\mathbf{E}}_{scat}(\mathbf{r}) = \tilde{\mathbf{G}}_p^{scat}(\mathbf{r},\mathbf{r}_0,\omega) \cdot \tilde{\mathbf{p}}_0, \tag{1}$$

where $\tilde{\mathbf{G}}_p^{scat}(\mathbf{r},\mathbf{r}_0,\omega)$ is the dyadic Green function for the scattered field describing the electromagnetic response of the whole environment (the vacuum and the nano-particle) at point $\mathbf{r}$. Here - and hereafter - we use Gaussian units. The total electric field is given by

$$\tilde{\mathbf{E}}_{tot}(\mathbf{r}) = \tilde{\mathbf{E}}_{scat}(\mathbf{r}) + \tilde{\mathbf{E}}_{inc}(\mathbf{r}), \tag{2}$$

where

$$\tilde{\mathbf{E}}_{inc}(\mathbf{r}) = \tilde{\mathbf{G}}_0(\mathbf{r},\mathbf{r}_0,\omega) \cdot \tilde{\mathbf{p}}_0, \tag{3}$$

and $\tilde{\mathbf{G}}_0(\mathbf{r},\mathbf{r}_0,\omega)$ is the free-space dyadic Green function [57]. The function $\tilde{\mathbf{G}}_p^{scat}(\mathbf{r},\mathbf{r}_0,\omega)$ is related to $\tilde{\mathbf{G}}_0(\mathbf{r},\mathbf{r}_0,\omega)$ by [57]

$$\tilde{\mathbf{G}}_p^{scat}(\mathbf{r},\mathbf{r}_0,\omega) = \int_P \tilde{\mathbf{G}}_0(\mathbf{r},\mathbf{r}_1,\omega)\tilde{\mathbf{T}}_p(\mathbf{r}_1,\omega)\tilde{\mathbf{G}}_0(\mathbf{r}_1,\mathbf{r}_0,\omega)\mathrm{d}^3\mathbf{r}_1, \tag{4}$$

where the scattering operator for the nano-particle is [57]

$$\tilde{\mathbf{T}}_p(\mathbf{r},\omega) = \tilde{\chi}_p(\mathbf{r},\omega)\mathbf{I} + \tilde{\chi}_p(\mathbf{r},\omega)\int_P \tilde{\mathbf{G}}_0(\mathbf{r},\mathbf{r}_1,\omega)\tilde{\mathbf{T}}_p(\mathbf{r}_1,\omega)\mathrm{d}^3\mathbf{r}_1, \tag{5}$$

and $\tilde{\chi}_p(\mathbf{r},\omega)$ is the (local) dielectric susceptibility of the nano-particle. Note that integrals in Eqs. (4) and (5) are restricted to the nano-particle volume, as $\tilde{\chi}_p$ vanishes outside it.

Here, attention is focused on the scattered field $\tilde{\mathbf{E}}_{scat}$ exactly at the dipole source position $\mathbf{r}_0$. Eqs. (4) and (5) are difficult to solve, and different approximations have been considered in the literature. For example, the nano-particle itself can be approximated as a point dipole [39]; however, this *dipole-dipole* approximation can be applied only for nano-particle-molecule distances larger than a few (i.e., two to three) radii of the metal nano-particle, otherwise the total decay rate is largely underestimated [58]. Higher multi-pole moments are needed for a correct description [58, 59], as is the case in the Gersten and Nitzan model [59, 60].

The underlying idea of the present work is to numerically approach the exact local field at the dipole position by solving the Maxwell's equations within the DDA framework. By solving in a self-consistent manner a system of $3N$-coupled complex equations, DDA gives N dipoles $\tilde{\mathbf{p}}_i$ describing the polarization of the target so that the scattered field experienced by the dipole [61] can be written as

$$\tilde{\mathbf{E}}_{scat}\left(\mathbf{r}_0\right) = \sum_{i=1}^{N}\tilde{\mathbf{G}}_0\left(\mathbf{r}_0,\mathbf{r}_i,\omega\right)\cdot\tilde{\mathbf{p}}_i, \qquad (6)$$

where $\tilde{\mathbf{p}}_i$ is located at $\mathbf{r}_i$.

In the weak-coupling interactions regime, the knowledge of the scattered field at $\mathbf{r}_0$ allows us to compute the irreversible enhancement of the total emission rate [62 - 65] or the total decay rate normalized to the free-space value [8, 57]

$$\frac{\Gamma}{\Gamma_0} = 1 + \frac{3}{2}\frac{q_0}{k^3\left|\tilde{\mathbf{p}}_0\right|^2}\mathrm{Im}\left[\tilde{\mathbf{p}}_0^*\cdot\tilde{\mathbf{E}}_{scat}\left(\mathbf{r}_0\right)\right], \qquad (7)$$

where Γ_0 is the total decay rate of a (classical) dipolar emitter with an intrinsic quantum yield q_0 i.e., corresponding to the total radiated power (P_0) of the dipole $\tilde{\mathbf{p}}_0$ in a vacuum, normalized to the energy

$$\Gamma_0 = \frac{1}{q_0}\frac{P_0}{\hbar\omega} = \frac{1}{3q_0\hbar}\left|\tilde{\mathbf{p}}_0\right|^2 k^3 . \qquad (8)$$

Note that in the case of a QE, $\tilde{\mathbf{p}}_0$ will be double the transition dipole moment between the ground-state and excited-state level [57].

Using Eq. (6) and the fact that the space-dyadic Green function is symmetric [66], we can rewrite Eq. (8) as

$$\frac{\Gamma}{\Gamma_0} = 1 + \frac{3}{2}\frac{q_0}{k^3\left|\tilde{\mathbf{p}}_0\right|^2}\sum_{i=1}^{N}\mathrm{Im}\left[\tilde{\mathbf{p}}_i\cdot\tilde{\mathbf{G}}_0\left(\mathbf{r}_i,\mathbf{r}_0,\omega\right)\cdot\tilde{\mathbf{p}}_0^*\right] . \qquad (9)$$

Eq. (9) can be further simplified assuming (as usual) that the external perturbing dipole $\tilde{\mathbf{p}}_0 = \mathbf{p}_0$ is real. Thus, from Eq. (3) we obtain

$$\frac{\Gamma}{\Gamma_0} = 1 + \frac{3}{2}\frac{q_0}{k^3\left|\mathbf{p}_0\right|^2}\sum_{i=1}^{N}\mathrm{Im}\left[\tilde{\mathbf{p}}_i\cdot\tilde{\mathbf{E}}_{inc}(\mathbf{r}_i)\right] , \qquad (10)$$

which involves only quantities readily available in DDA.

It has been largely proved that the change expressed by Eq. (7) and known as the 'Purcell effect' [1] can be ascribed to the modifications of both the radiative decay rate due to photon emission and the non-radiative decay rate due to energy dissipation in the environment [67 - 70]. For emitters close to metal surfaces, both rates can be enhanced. If the nano-particle is dissipative, Γ/Γ_0 is the sum of the intrinsic non-radiative term $\Gamma_{NR,0}/\Gamma_0 = (1-q_0)$, the radiative decay enhancement (Γ_R/Γ_0) and the quenching rate enhancement induced by the lossy environment (Γ_{NR}/Γ_0) [71, 15, 16], i.e.,

$$\frac{\Gamma}{\Gamma_0} = \left(1 - q_0\right) + \frac{\Gamma_R}{\Gamma_0} + \frac{\Gamma_{NR}}{\Gamma_0} . \qquad (11)$$

According to semi-classical theory [59], the non-radiative decay rate is $\Gamma_{NR} = P_{abs}/\hbar\omega$, where P_{abs} is the (time-averaged) power absorbed by the nano-particle

$$\begin{aligned}P_{abs} &= \int_P \frac{\omega}{2}\mathrm{Im}\left[\tilde{\chi}_p\left(\mathbf{r}\right)\right]\left|\tilde{\mathbf{E}}_{tot}\left(\mathbf{r}\right)\right|^2 \mathrm{d}^3\mathbf{r} \\ &= \frac{\omega}{2}\sum_{i}^{N}V_c\,\mathrm{Im}\left[\tilde{\chi}_p\left(\mathbf{r}_i\right)\right]\left|\tilde{\mathbf{E}}_{tot}\left(\mathbf{r}_i\right)\right|^2 .\end{aligned} \qquad (12)$$

In Eq. (12), we discretized the integral over the nano-particle: the summation is done on the N dipoles' contributions, V_c is the volume of each cubic element, and $\tilde{\mathbf{E}}_{tot}(\mathbf{r}_i)$ is the total internal electric field at position $\mathbf{r}_i$.

The normalized non-radiative decay rate Γ_{NR} thus becomes

$$\frac{\Gamma_{NR}}{\Gamma_0} = \frac{3q_0}{2k^3\left|\tilde{\mathbf{p}}_0\right|^2}\left(\sum_{i=1}^{N}\mathrm{Im}\left[\tilde{\chi}_p\left(\mathbf{r}_i\right)\right]\left|\tilde{\mathbf{E}}_{tot}\left(\mathbf{r}_i\right)\right|^2\cdot V_c\right) \qquad (13)$$

and by using the relation $\tilde{\mathbf{p}}_i = V_c\chi_p(r_i)\tilde{\mathbf{E}}_{tot}(r_i)$ [31],

$$\frac{\Gamma_{NR}}{\Gamma_0} = \frac{3q_0}{2\left|\mathbf{p}_0\right|^2 k^3}\sum_{i=1}^{N}\mathrm{Im}\left[\tilde{\mathbf{p}}_i\cdot\tilde{\mathbf{E}}_{tot}^*(\mathbf{r}_i)\right] . \qquad (14)$$

On the other hand, the radiative decay rate can be computed considering the power radiated in the far-field. In the far-field zone, the radiated electric field ($\tilde{\mathbf{E}}_{rad}$), the radiated magnetic field ($\tilde{\mathbf{H}}_{rad}$) and the radiated Poynting vector ($\tilde{\mathbf{S}}_{rad} = (c/8\pi)\tilde{\mathbf{E}}_{rad} \times \tilde{\mathbf{H}}_{rad}^{*}$), can be computed as

$$\tilde{\mathbf{E}}_{rad}(\mathbf{r}) = \frac{\exp(ikr)}{-ikr}\tilde{\mathbf{F}}(\hat{\mathbf{r}}) \ , \tag{15}$$

$$\tilde{\mathbf{H}}_{rad}(\mathbf{r}) = \frac{\exp(ikr)}{-ikr}\hat{\mathbf{r}} \times \tilde{\mathbf{F}}(\hat{\mathbf{r}}) \ , \tag{16}$$

$$\tilde{\mathbf{S}}_{rad}(\mathbf{r}) = \frac{c}{8\pi k^2 r^2}\hat{\mathbf{r}}\left|\tilde{\mathbf{F}}(\hat{\mathbf{r}})\right|^2 \ , \tag{17}$$

where $\hat{\mathbf{r}} = \mathbf{r}/r$ and the scattering amplitude

$$\tilde{\mathbf{F}}(\hat{\mathbf{r}}) = -ik^3\left(\bar{\mathbf{I}} - \hat{\mathbf{r}}\hat{\mathbf{r}}\right)\left(\mathbf{p}_0\exp\left(-ikr_0\cdot\hat{\mathbf{r}}\right) + \right. \\ \left. + \sum_{i=1}^{N}\tilde{\mathbf{p}}_i\exp(-ik\mathbf{r}_i\cdot\hat{\mathbf{r}})\right) \tag{18}$$

contain N polarizable points $\tilde{\mathbf{p}}_i$ as well as the external source $\mathbf{p}_0$. The radiative decay rate is thus:

$$\Gamma_R = \frac{\int_S Re\left[\tilde{\mathbf{S}}_{rad}(\mathbf{r})\right]\cdot\hat{\mathbf{n}}dS}{\hbar\omega} = \frac{1}{8\pi k^3\hbar}\int_{\Omega}\left|\tilde{\mathbf{F}}(\hat{\mathbf{r}})\right|^2 d\Omega \ , \tag{19}$$

where S is the surface in the far-field and Ω is the solid-angle. Clearly, if we consider only the dipole $\mathbf{p}_0$ in Eq. (18), the integral over Ω is $\left(k^6 8\pi/3\right)|\mathbf{p}_0|^2$ and Eq. (8) is obtained. The normalized radiative decay rate is thus

$$\frac{\Gamma_R}{\Gamma_0} = \frac{3q_0}{8\pi k^6\left|\mathbf{p}_0\right|^2}\int_{\Omega}\left|\tilde{\mathbf{F}}(\hat{\mathbf{r}})\right|^2 d\Omega \ . \tag{20}$$

Eq. (20) is difficult to compute numerically due to the integral over Ω. Beyond this *direct* method, which does not involve any limitation or approximation, it is also possible to acquire this quantity using Eq. (11), i.e., considering Γ and Γ_{NR} in Eq. (7) and Eq. (13), respectively (we will refer to this method as the *indirect* one). Alternatively, if all the phases in Eq. (18) are neglected, i.e., if the relative distances between the points $\mathbf{r}_0, \mathbf{r}_1, ..., \mathbf{r}_N$ (i.e., the particle size and the particle-external dipole distance) are much smaller than the wavelength of the emitted light, we simply obtain

$$\frac{\Gamma_R}{\Gamma_0} \approx \frac{1}{\left|\mathbf{p}_0\right|^2}\left|\sum_{i=1}^{N}\tilde{\mathbf{p}}_i + \mathbf{p}_0\right|^2 \ , \tag{21}$$

which represents the enhancement of the total dipole. While (Eq. 7) and (Eq. 13) always give an exact expression of the total non-radiative decay rate, within the limit of a fine discretization, and we underline that the radiative contribution calculated with Eq. (21) is only valid in the cases of small nano-particles and a few nanometre emitter-metal distances [32]. Phase shifts and interference effects could affect the results under the regime of large distances.

In the following paragraphs, we report the radiative decay rate perturbations calculated with the indirect method or - equivalently - by the difference, although we have recently shown that for small nano-particles such as those considered here, Eq. (21) gives values which correspond almost exactly to the differences between the total decay rate (Eq. 7) and the non-radiative decay rate (Eq. 13) [32]. In this approximation, once the radiative and total decay rates are known, the quantum yield or quantum efficiency of the complete system can be calculated by the general formula

$$q = \frac{\Gamma_R/\Gamma_0}{\left(\Gamma_R + \Gamma_{NR} + \Gamma_{NR,0}\right)/\Gamma_0} = \frac{\Gamma_R/\Gamma_0}{\Gamma/\Gamma_0 + \left(1 - q_0\right)}. \tag{22}$$

The decay rate perturbations reported here are the result of extreme interest in describing the changes induced by an antenna on the decay dynamics of a point-like emitter in the regime of weak coupling. Furthermore, by taking advantage of these as well as photonic Lamb shift - which can be easily calculated in this framework - DDA offers a useful tool for a complete description of strong coupling interactions. It has been recently shown, in fact, that if we combine DDA with a quantum electrodynamics treatment of light-matter interaction, we can calculate the dipole spectrum and the power spectrum emitted to the far-field by a point-like dipole placed in proximity to plasmonic nano-antennas and without any limitation on the geometry of the system [34, 72].

3. Reliability of DDA Numerical Results

Here, version 1.3 of the open source code ADDA developed by M. Yurkin and A. G. Hoekstra [35] is used. ADDA's main feature is the ability to run on a multiprocessor system by parallelizing a single DDA simulation. For each exciting frequency, the scatterer is partitioned in slices parallel to the xy-plane so that the run-time is significantly reduced [73]. As to what concerns the choice of the inter-dipole distance or discretization parameter d_{int} (which in DDA represents the side of the elementary cube), the possibility of quickly ensuring convergence depend upon the size and the shape of the considered nano-structure. The results reported in the next sections are obtained by setting $d_{int} = 1/16$ nm.

Stefania D'Agostino, Fabio Della Sala and Lucio Claudio Andreani: 5
Perturbations of Dipole Decay Dynamics Induced by Plasmonic Nano-antennas – A Study within the
Discrete Dipole Approximation

For spherically-shaped nano-particles, as well as for sharp objects, i.e., the nano-cones analysed in this work, special attention should be paid to the convergence problem. For spherically-shaped nano-particles, the adopted prescription for the discretization parameter $d_{int} = 1/16$ nm is proven to be good enough by recurring to a comparison with the analytical results. In Fig. 1 and 2, a comparison between the numerical and the analytical results is shown for the benchmark cases of a 10 nm Ag nano-sphere and a 10 nm Ag nano-shell with a 2 nm wall-thickness, respectively. The DDA decay rate perturbations are compared with the results obtained within exact electrodynamics theory (EET) [74] for the sphere (Fig. 1) and the recursive transfer-matrix (RTM) solutions [75 - 77] for the nano-shell (Fig. 2). As can be noted in Fig. 1 and Fig. 2, the agreement between numerical and analytical decay rates as functions of the emitter wavelength (total decay rates in panels b) and dipole distance (total, radiative and non-radiative decay rates in panel c), turns out to be almost perfect for both the orientations, parallel and perpendicular to the metallic surface.
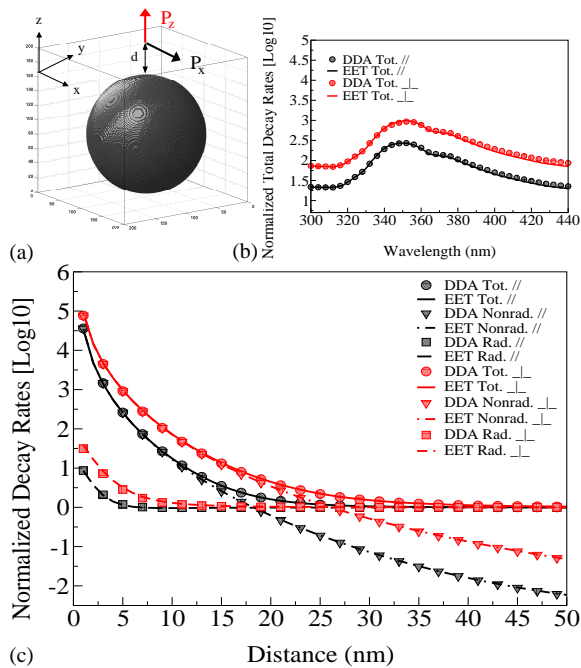
Figure 1. (a) Sketch of a 10 nm-diameter Ag sphere excited by a dipole-oriented in parallel (P_x) or perpendicular (P_z) to the surface. (b) DDA and EET normalized total decay rates calculated for the system in (a) for a distance from the surface $d = 5$ nm. (c) DDA and EET normalized total, radiative and non-radiative decay rates calculated for the same system for $\lambda_{exc} = 354$ nm. The analytical values are represented with lines while the numerical ones with symbols. The inter-dipole distance used is $d_{int} = 1/16$ nm and the values are reported in a decimal logarithmic scale.

In all the DDA simulations reported here (the benchmark and the new cases in the Sec. IV), the metal is described using the experimental dielectric function of Palik [78] and q_0 is assumed to be unity unless otherwise specified.
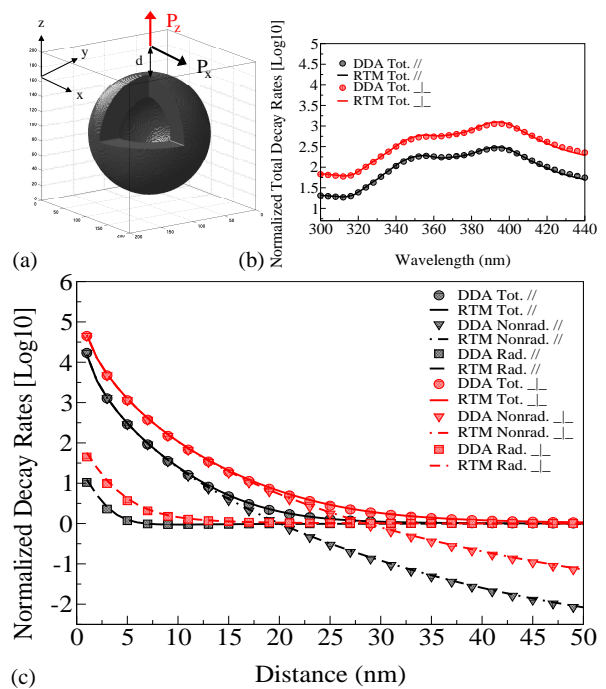
Figure 2. (a) Sketch of a 10 nm-diameter Ag shell with a wall thickness of 2 nm, excited by a dipole oriented in parallel (P_x) or perpendicular (P_z) to the surface. (b) DDA and RTM normalized total decay rates calculated for the system in (a) for a distance from the surface $d = 5$ nm. (c) DDA and RTM normalized total, radiative and non-radiative decay rates calculated for the same system for $\lambda_{exc} = 394$ nm nm. The analytical values are represented with lines while the numerical values with symbols. The inter-dipole distance used is $d_{int} = 1/16$ nm and the values are reported in a decimal logarithmic scale.

4. Results: Beyond Analytically-solved Shapes

4.1 Total Decay Rates

In Fig. 3, the total decay rates normalized to the dipole free-space decay rate (also called 'normalized 'decay rates) are reported as a function of the wavelength for three differently-shaped nano-particles: a 10 nm Ag nano-sphere, a 10 nm Ag nano-shell with a 2 nm wall thickness (the same as Sec. II) and a 20 nm-high Ag cone with a negligible curvature radius and a semi-aperture of $\pi/13$ rad. The decay rates of a cone cannot be computed analytically, and thus a fully numerical approach (such as DDA) is required. In Fig. 3, we consider both the parallel (panels a,b,c) and perpendicular (panels d,e,f) orientations for three different emitter distances ($d = 2, 5, 10$ nm).

While the optical responses of the sphere and the nano-shell give results that are very similar to each other, regarding what concerns their dependence on the dipole orientation as well as the dipole distance, the behaviour of the analysed sharp nano-cone is instead quite peculiar.

Concerning the effects of the dipole orientation, the sphere and the nano-shell both present similar spectra (i.e., they peaked around 350-400 nm) by moving from a parallel orientation of the dipole to a perpendicular one, the only
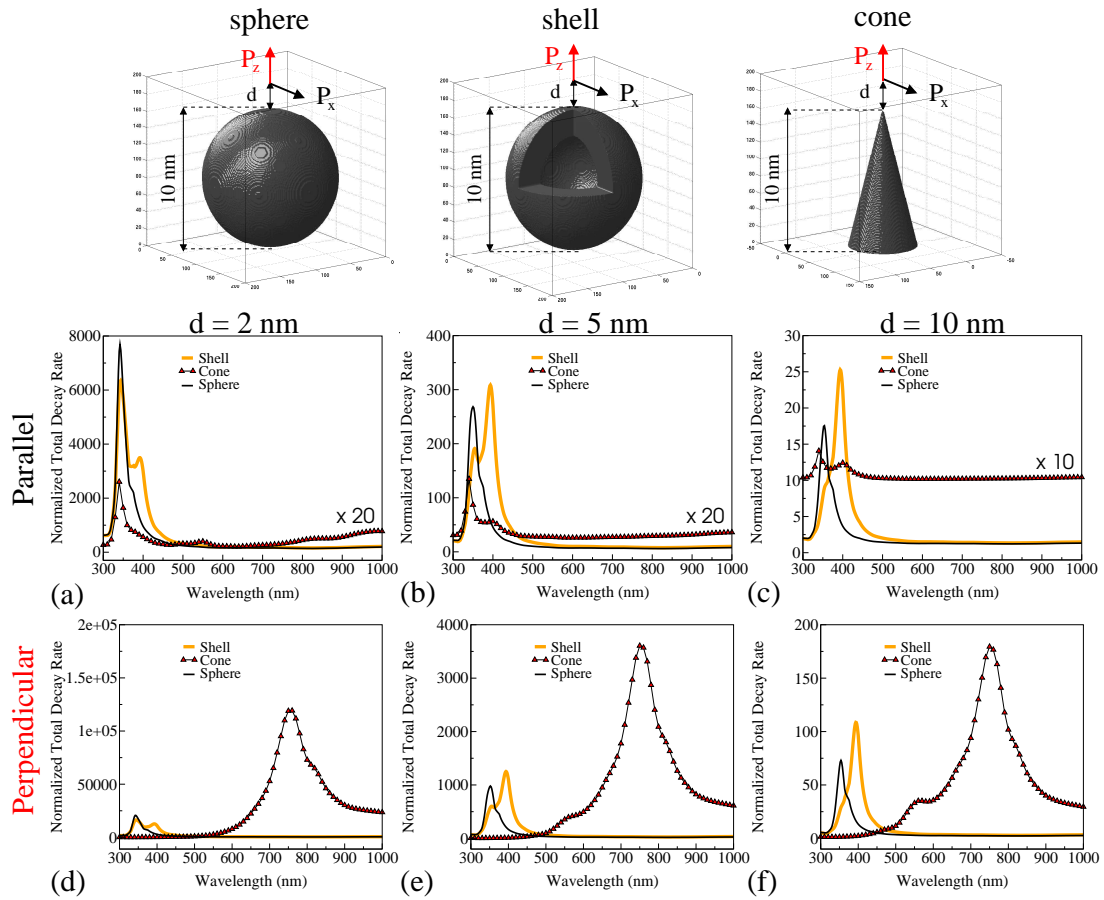
Figure 3. Normalized total decay rates calculated for a dipole oscillating in parallel (a,b,c) and perpendicular (d,e,f) to the nano-particles sketched on the top (a 10 nm-diameter Ag sphere, a 10 nm-diameter Ag shell with a wall thickness of 2 nm, and a 10 nm-high Ag cone with an aperture of $\pi / 13$ rad). The decay rate perturbations are reported for several distances of the dipole from the metallic surface: 2 nm (a,d), 5 nm (b,e) and 10 nm (c,f). For graphical readability, the values relative to the cone were multiplied by an extra factor in panels (a-b-c).

difference being the greater intensity of the decay rate in the latter case. For both orientations, a peak at 342 nm and the shoulder on the low-energy side for the sphere, as well as the two resonances at 344 nm and 393 nm for the shell, are clearly visible in the decay rate spectra (Fig. 3).

The nano-cone response presents significant sensitivity to the dipole orientation. As can be observed in Figs. 3a and 3d (i.e., considering the case of a 2 nm distance), the two decay spectra of the nano-cone obtained for the parallel and the perpendicular orientations are substantially different. For the parallel case, a small peak appears at 340 nm, while for the perpendicular orientation we can observe a strong resonance at 760 nm: the values for the maxima go from about 130 for the parallel case to about 120000 for the perpendicular one. Thus, the perpendicular orientation strongly dominates the decay rate variations. For practical applications, this important increase in the decay rate could strongly decrease the lifetimes of those emitters which have a typical lifetime of 10 ns, this being desirable to take full advantage of the new generation of mode-locked lasers with high repetition rates. As discussed in Ref. [32], the resonance at 760 nm looks like a dipole mode, which can be excited by both near- and far-source radiations.

Concerning the effects related to the dipole distance, besides the huge spread of the maximum values resulting from moving from the spherical nano-particles to the cone, and as registered for all the analysed distances, for the case of the cone we note a counter-intuitive trend with regard to distance. By moving away from the tip, the spectrum becomes broader, with a shoulder on the short-wavelength side of the dipolar resonance until a second peak appears at 560 nm. For larger distances, a third peak rises around 490 nm, and for a 50 nm-distant emitter, the field induced by the dipole behaves like that induced by a plane wave with the same polarization properties (z polarization) [32]. This dependence of the spectrum on the emitter-metal separation seems counter-intuitive and is very interesting if we compare it with the trend obtained for the sphere and the nano-shell. For the spherically-shaped nano-particles analysed here, as well as for the major part of few-nano-metre plasmonic nano-particles, uniform fields can excite only the dipolar surface plasmon mode, while strongly variable fields are able to excite higher-order modes associated with more complex electronic charge oscilla-tions. A full analysis of this effect, together with the charge distribution of the modes, is given in Ref. [32].

Stefania D'Agostino, Fabio Della Sala and Lucio Claudio Andreani:
Perturbations of Dipole Decay Dynamics Induced by Plasmonic Nano-antennas – A Study within the
Discrete Dipole Approximation

7
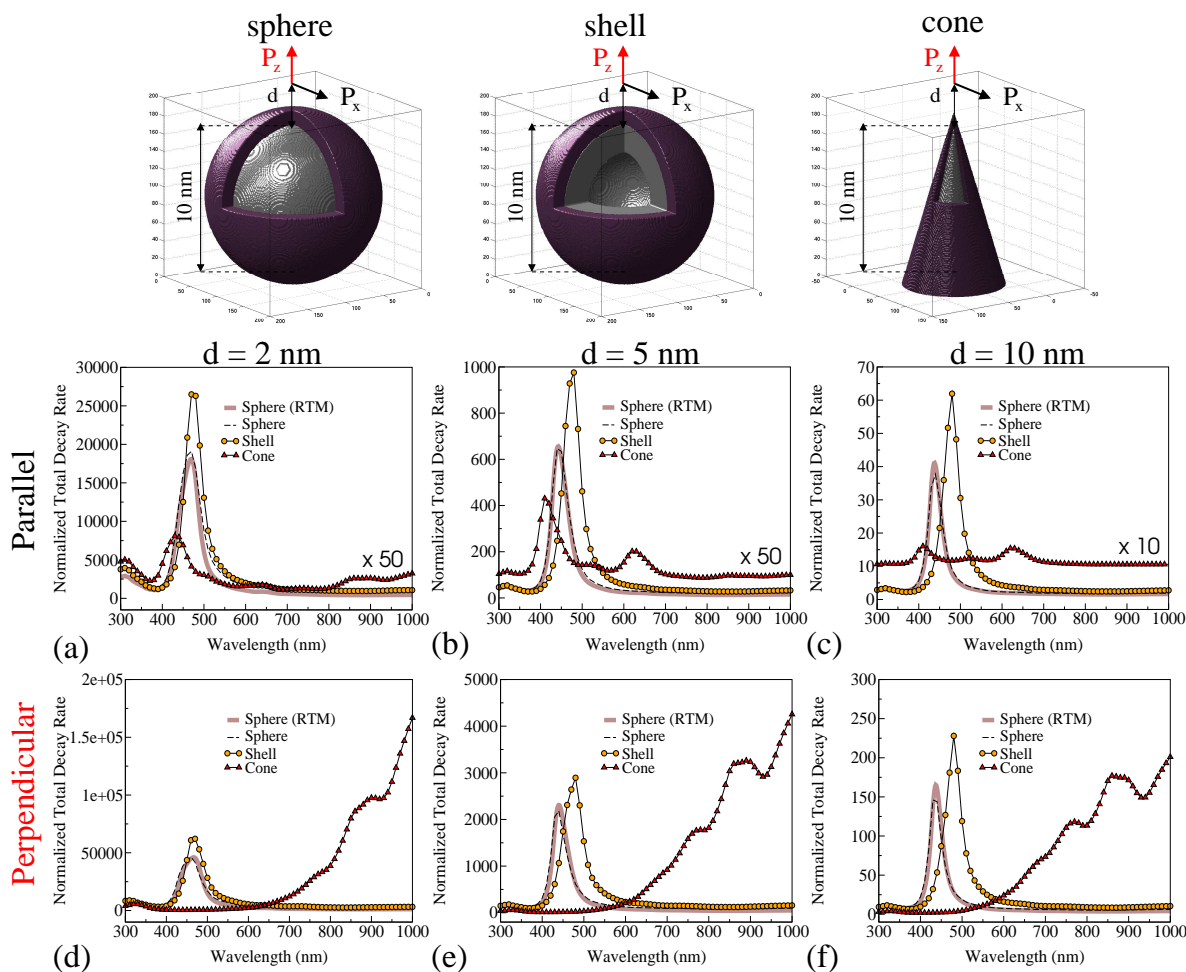
Figure 4. Normalized total decay rates calculated for a dipole oscillating in parallel (a,b,c) and perpendicular (d,e,f) to the nano-particles in Fig. 3 but covered with a thin Ag_2O layer (1 nm) (sketched on the top). The decay rate perturbations are reported for several distances of the dipole from the metallic surface: 2 nm (a,d), 5 nm (b,e) and 10 nm (c,f). For the sphere, the curves obtained analytically with the RTM approach are also reported for a comparison (yellow solid lines). For graphical readability, the values relative to the cone were multiplied by an extra factor in panels (a-b-c).

The results of Fig. 3 therefore show that a small, conically-shaped nano-particle, like the one analysed here, can support several plasmonic resonances in the VIS spectral range, and that the higher-order resonances can be excited, provided that the distance between the dipole and the tip is properly tailored. This can be very useful to get information on the metal-emitter distance in experimental set-ups: in a scanning microscopy configuration, the distance between the tip and the sample could in fact be determined from the spectral dependence of the measured decay rates.

The appearance of higher-order modes with the increasing distance of the emitter dipole from the cone tip is then further evidenced by covering the nano-particle with a thin Ag_2O layer (1 nm), see Fig. 4. Here, the complex refractive index of the Ag_2O layer is taken by a spectroscopic ellipsometric study of the optical properties of Ag_2O-deposited films [79].

By covering the nano-cone with a silver oxide layer, in fact, we can note that for the same distance of the emitter from

the metallic surface (here, the distance has to be considered from the metal surface and not from the outer, oxidated surface), we have more distinguishable peaks even if shifted in the red part of the spectral range, similarly to as is shown in [80] (see Fig. 4-d,e,f). The Ag_2O's ability to absorb radiation becomes responsible for huge internal fields inside the oxide layer, this producing an important enhancement of the non-radiative decay channel of the dipole radiation. The maxima values obtained for the total decay rate, reported in Fig. 4, thus appear significantly higher than those achieved in the bare nano-particles case (Fig. 3). The presence of an Ag_2O layer thus enhances the local field in proximity of the metallic surface, this allowing for a better coupling of radiation with the plasmonic modes. In the cases of the sphere and the nano-shell, the same field confinement around the Ag surface leads to a higher coupling of radiation with the lower-energy modes in Fig. 3, and to a complete redistribution of the spectral intensity. Once again, we want to stress the good agreement between the numerical results obtained for the oxidated sphere and the analytical ones calculated with the RTM

method [75 - 77] by assuming a 5 nm-radius Ag core and 1 nm-thick Ag_2O shell (yellow solid lines in Fig. 4).

Finally, we can note that in both Fig. 3 and Fig. 4, the normalized total decay rate does not vanish for long wavelengths. This is more evident in the case of the cone, but it is also true for the sphere and the shell. In fact, all the reported spectra are dominated by the non-radiative contribution (due to the small emitter distance, see also Figs. 1 and 2), and the non-radiative contribution diverges as λ^3 for very large λ [59].

4.2 Internal Fields and Quantum Yields

The internal fields for the resonant wavelengths, with and without an oxide covering layer, are reported in Fig. 5. The field maps are related to the total decay rate resonances in Fig. 3 and 4. As to the field's dependence on the shape, we can observe, once again, the large difference between the spherically-shaped nano-particles and the cone by moving from a perpendicular to a parallel dipole orientation. These maps confirm, in fact, the higher sensitivity of a conical shape to the dipole orientation of the emitting dipole: for the sphere (panel 1) and the nano-shell (panels 2), by moving from the left column to the right column, we have substantially the same internal fields, whereas for the cone (panel 3) we note a sort of 'shutting down' of the resonance with the field switching off from the perpendicular to the parallel case.

Concerning the role of Ag_2O, in all the cases we can observe a significant enhancement of the internal field inside the metal when calculated in the presence of the thin oxide layer.

The field confinement due to the oxide and the derivative increase of the internal field shown in Fig. 5 thus becomes responsible for an important growth of the non-radiative decay channel in terms of the spontaneous emission rate for the dipole placed near the oxidated structures. Through Eq. (13), it is a simple matter to understand how higher internal fields inside the nano-antennas produce larger non-radiative decay rates. As a consequence, by moving from a bare Ag nano-particle to an oxidated one, we expect an evident decrease of the quantum yield (the increase in the radiative decay rates not being enough to compensate the losses inside the metal). The quantum yield-lowering is very visible in Fig. 6, where the dipole distance is fixed at 5 nm from the nano-particle surface. If the presence of oxide produces a significant decrease of the quantum efficiency q in all the cases, again the difference between spherically- and conically-shaped nano-particles should be noted. While the wavelength dependence of q for the sphere and the nano-shell spectra remain unchanged for both orientations, with only an expected small reduction of q in the perpendicular case, the response of the oxidated cone is completely different. By moving from a parallel to a perpendicular orientation, important changes in q are

registered in terms of both the spectral position and intensity of the peaks.
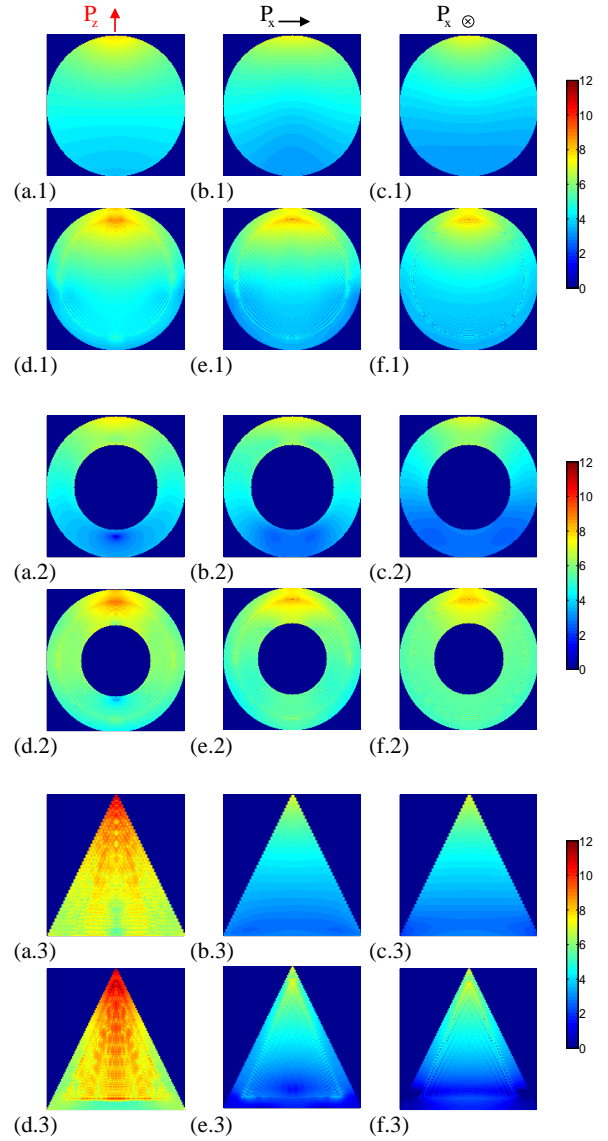
Figure 5. The modulus squared of the internal local field without (a,b,c) and with (d,e,f) a thin oxide layer (the values are in a decimal logarithmic scale). The upper panels represent the sphere, the middle panels the shell, the bottom panels the cone. The dipole is assumed to oscillate perpendicularly (a,d) and in parallel (b,c,e,f) to the surface at 2 nm from the metal. Resonant wavelengths: 342 nm (a.1,b.1,c.1), 460 nm (d.1) and 470 nm (e.1,f.1); 344 nm (a.2,b.2,c.2) and 470 nm (d.2,e.2,f.2); 760 nm (a.3), 340 nm (b.3,c.3), 1000 nm (d.3) and 430 nm (e.3,f.3).

Finally, we can note that all the quantum yields reported in Fig. 6 are lower than the intrinsic quantum yield (we assumed q_0=0.1). In Fig. 7, the quantum yield is calculated in the RTM framework and reported as a function of the emitting wavelength and the nano-sphere diameter to shed light on the effects of antenna-dimension without or with a 1 nm-thick oxide layer (to be compared with those obtained for 10 nm spheres in panels (a) and (d) of Fig. 6). For the parallel case, the presence of the antenna is always
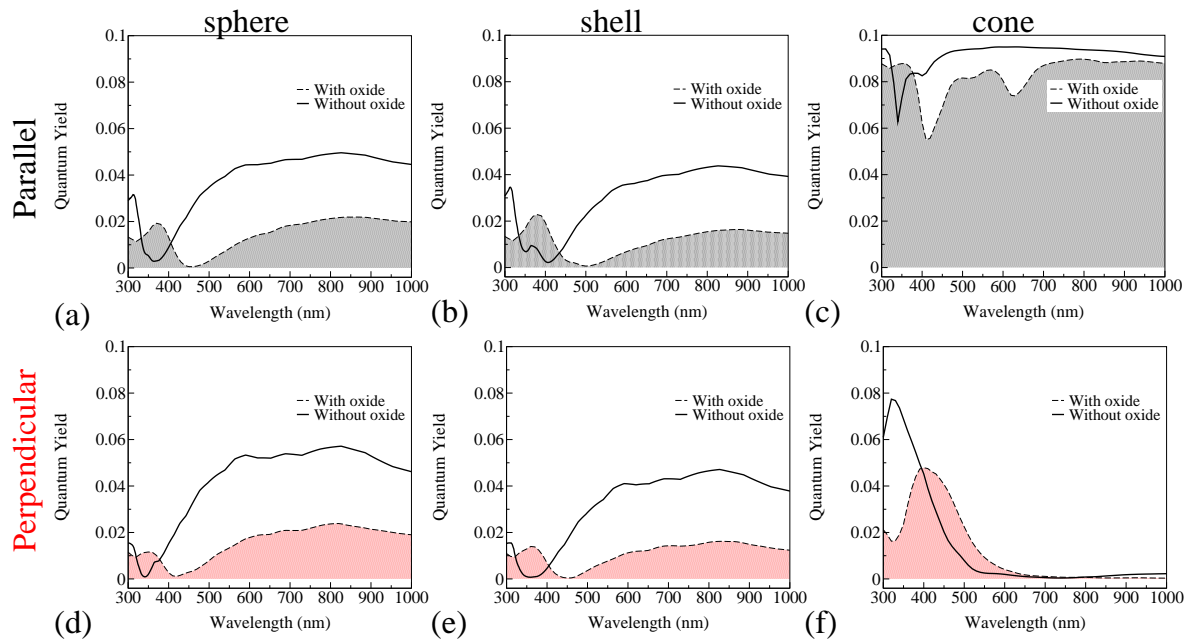
Figure 6. Quantum yield calculated for a dipole oscillating parallel (a,b,c) and perpendicular (d,e,f) to the sphere, the shell and the cone with and without a thin oxide layer (1 nm). The distance of the emitting dipole from the metallic surface is fixed to 5 nm and the intrinsic quantum yield is assumed to be equal to $q_0 = 0.1$.

disadvantageous due to making the dipole quantum efficiency lower than its intrinsic value, whereas the antenna efficiency in the case of a dipole oscillating along the radial direction increases up to 0.25 for very large nanoparticle diameters ($D > 160$ nm). Again, these enhancements gives results less than those which can be achieved for equivalently-sized bare Ag nano-spheres.

Figure 7. Quantum yield maps calculated in the RTM framework for a dipole (with an intrinsic quantum yield $q_0 = 0.1$) oscillating parallel (a,c) and perpendicular (b,d) to a several-diameter Ag nano-sphere without (a,b) and with a 1 nm-thick Ag_2O layer (c,d). The dipole distance is fixed at 5 nm from the metallic surface, as in Fig. 6.

5. Conclusions

In conclusion, in this work we have summarized the basic theoretical principles and the potentialities of a DDA-based approach for the study of the perturbations induced on the dipole decay dynamics by plasmonic nano-antennas of arbitrary shape and composition. The analysis gives the expressions to numerically compute the total, radiative and non-radiative decay rates normalized to the free-space dipole decay rate. The reliability of the method is also proved by reporting the comparison of the DDA results and the numerical ones obtained for the benchmark case of analytically-solved shapes (e.g., spheres and nano-shells). Concerning the results, the peculiar behaviour of a metallic sharp-tip is evidenced by comparing this with that of spherically-shaped nano-particles. In particular, two phenomena are stressed, i.e., the extreme sensitivity of conically-shaped nano-particles on the dipole orientation, and a counter-intuitive trend of spectra with the increasing distance of the metal from the source of radiation. The effects of a thin oxide layer on the perturbations induced by the same Ag nano-antennas on the dipole decay dynamics are also shown. Beyond a red-shift of the major resonances, the field localization around the metal due to the oxide layer produces important changes in the total decay-rate spectra. These can be summarized in the disappearance of the peaks at higher energies for the spherically-shaped nano-particles and in a stronger coupling of dipole radiation to higher-order peaks for the cone. We believe that these results contribute to attesting the importance of the numerical engineering of decay rates exploiting surface plasmon resonances, and in view of the

considered experimental control of decay processes in both weak and strong coupling regimes of light-matter interactions.

6. Acknowledgements

7. References

[1] Purcell EM (1946) Spontaneous emission probabilities at radio frequencies. Phys. Rev. 69: 681.

[2] Ruppin R (1982) Decay of an excited molecule near a small metal sphere. J. Chem. Phys. 76: 1681-1684.

[3] Chew H (1987) Transition rates of atoms near spherical surfaces. J. Chem. Phys. 87: 1355-1360.

[4] Leung PT, George TF (1987) Dynamical analysis of molecular decay at spherical surfaces. J. Chem. Phys. 87: 6722-6724.

[5] Dulkeith E, Morteani AC, Niedereichholz T, Klar TA, Feldmann J, Levi SA, van Veggel FCJM, Reinhoudt DN, Möller M, Gittins DI (2002) Fluorescence quenching of dye molecules near gold nanoparticles: Radiative and nonradiative effects. Phys. Rev. Lett. 89: 203002-1/4.

[6] Anger P, Bharadwaj P, Novotny L (2006) Enhancement and quenching of single-molecule fluorescence. Phys. Rev. Lett. 96: 113002-1/4.

[7] Hümmer T, García-Vidal FJ, Martín-Moreno L, Zueco D (2013) Weak and strong coupling regimes in plasmonic QED. Phys. Rev. B 87: 115419-1/16.

[8] Novotny L (1996) Single molecule fluorescence in inhomogeneous environments. Appl. Phys. Lett. 69: 3806-3808.

[9] Lakowicz JR, Shen Y, D'Auria S, Malicka J, Fang J, Gryczynski Z, Gryczynski I (2002) Radiative decay engineering. Analytical Biochemistry 301: 261-277.

[10] Lakowicz JR (2005) Radiative decay engineering 5: metal-enhanced fluorescence and plasmon emission. Analytical Biochemistry 337: 171-194.

[11] Kühn S, Hakanson U, Rogobete L, Sandoghdar V (2006) Enhancement of single-molecule fluorescence using a gold nanoparticle as an optical nanoantenna. Phys. Rev. Lett. 97: 017402-1/4.

[12] Schuller JA, Barnard ES, Cai WS, Yun YC, White JS, Brongersma ML (2010) Plasmonics for extreme light concentration and manipulation. Nat. Mater. 9: 193-204.

[13] Anger P, Bharadwaj P, Novotny L (2006) Enhancement and quenching of single-molecule fluorescence. Phys. Rev. Lett. 96: 113002-1/4.

[14] Muskens OL, Giannini V, Sànchez Gil JA, Gòmez Rivas J (2007) Strong enhancement of the radiative decay rate of emitters by single plasmonic nanoantennas. Nano Lett. 7: 2871-2875.

[15] Mertens H, Koenderink AF, Polman A (2007) Plasmon-enhanced luminescence near noble-metal nanospheres: comparison of exact theory and an improved Gersten and Nitzan model. Phys. Rev. B 76: 115123-1/12.

[16] Ford GW, Weber WH (1984) Electromagnetic interactions of molecules with metal surfaces. Phys. Rep. 113: 195-287.

[17] Taminiau TH, Stefani FD, Segerink FB, van Hulst NF (2008) Optical antennas direct single-molecule emission. Nat. Photon. 2: 234-237.

[18] Kinkhabwala A, Yu Z, Fan S, Avlavesich Y, Müllen K, Moerner WE (2009) Large single-molecule fluorescence enhancements produced by a bowtie nanoantenna. Nat. Photon. 3: 654-657.

[19] Chang DE, Sorensen AS, Demler EA, Lukin MD (2007) A single-photon transistor using nanoscale surface plasmons. Nature Phys. 3: 807-812.

[20] Muhlschlegel P, Eisler HJ, Martin OJF, Hecht B, Pohl DW (2005) Resonant optical antennas. Science 308: 1607-1609.

[21] Metiu H (1984) Surface enhanced spectroscopy. Prog. Surf. Sci. 17: 153-320.

[22] Zhang Y, Zhang R, Wang Q, Zhang Z, Haibo Z (2010) Fluorescence enhancement of quantum emitters with different energy systems near a single spherical metal nanoparticle. Opt. Expr. 18: 4316-4328.

[23] Savage KJ, Hawkeye MM, Esteban R, Borisov AG, Aizpurua J, Baumberg JJ (2012) Revealing the quantum regime in tunnelling plasmonics. Nature 491: 574-577.

[24] Esteban R, Borisov AG, Nordlander P, Aizpurua J (2012) Bridging quantum and classical plasmonics with a quantum-corrected model. Nat. Commun. 3: 825-1/9.

[25] Marinica DC, Kazansky AK, Nordlander P, Aizpurua J, Borisov AG (2012) Quantum plasmonics: nonlinear effects in the field enhancement of a plasmonic nanoparticle dimer. Nano Lett. 12: 1333-1339.

[26] Marinica DC, Lourencì§o-Martins H, Aizpurua J, Borisov AG (2013) Plexciton quenching by resonant electron transfer from quantum emitter to metallic nanoantenna. Nano Lett. 13: 5972-5978.

[27] Miertus S, Scrocco E, Tomasi J (1981) Electrostatic interaction of a solute with a continuum. A direct utilization of ab initio molecular potentials for the provision of solvent effects. J. Chem. Phys. 55: 117-129.

Stefania D'Agostino, Fabio Della Sala and Lucio Claudio Andreani: Perturbations of Dipole Decay Dynamics Induced by Plasmonic Nano-antennas – A Study within the Discrete Dipole Approximation

11

[28] Corni S, Tomasi J (2002) Excitation energies of a molecule close to a metal surface. J. Chem. Phys. 117: 7266-7278.

[29] Castanié E, Boffety M, Carminati R (2010) Fluorescence quenching by a metal nanoparticle in the extreme near-field regime. Opt. Lett. 35: 291-293.

[30] Draine BT, Flatau PJ (1994) Discrete-dipole approximation for scattering calculations. J. Opt. Soc. Am. A 11: 1491-1499.

[31] Yurkin MA, Hoekstra AG (2007) The discrete dipole approximation: an overview and recent developments. J. Quant. Spectrosc. Radiat. Transfer 106: 558-589.

[32] D'Agostino S, Della Sala F, Andreani LC (2013) Dipole-excited surface plasmons in metallic nanoparticles: an engineering of decay dynamics within the discrete Dipole Approximation. Phys. Rev. B 87: 205413.

[33] D'Agostino S, Della Sala F, Andreani LC (2013) Dipole Decay Rates Engineering via Silver Nanocones. Plasmonics 8: 1079-1086.

[34] D'Agostino S, Alpeggiani F, Andreani LC (2013) Strong Coupling between a dipole emitter and localized plasmons: enhancement by sharp silver tips. Opt. Expr. 21: 27602-27610.

[35] Yurkin MA, Hoekstra AG (2011) The discrete-dipole-approximation code ADDA: capabilities and known limitations. J. Quant. Spectrosc. Radiat. Transfer 112: 2234-2247. Code available at http://code.google.com/p/a-dda/

[36] Sipe JE (1987) New Green-function formalism for surface optics. J. Opt. Soc. Am. B 4: 481-489.

[37] Vandenbem C, Brayer D, Froufe-Pérez LS, Carminati R (2010) Controlling the quantum yield of a dipole emitter with coupled plasmonic modes. Phys. Rev. B 81: 085444.

[38] Vandenbem C, Froufe-Perez LS, Carminati R (2009) Fluorescence signal of a single emitter coupled to a nanoparticle through a plasmonic film. J. Opt. A: Pure Appl. Opt. 11: 114007.

[39] Carminati R, Greffet JJ, Henkel C, Vigoureux JM (2006) Radiative and non-radiative decay of a single molecule close to a metallic nanoparticle. Opt. Comm. 261: 368-375.

[40] Giannini V, Sànchez-Gil JA, Muskens OL, Gómez Rivas J (2009) Electrodynamic calculations of spontaneous emission coupled to metal nanostructures of arbitrary shape: nanoantenna-enhanced fluorescence. J. Opt. Soc. Am. B 26: 1569-1577.

[41] Froufe-Pérez LS, Carminati R (2008) Controlling the fluorescence lifetime of a single emitter on the nanoscale using a plasmonic superlens. Phys. Rev. B 78: 125403.

[42] Froufe-Pérez LS, Carminati R (2008) Lifetime fluctuations of a single emitter in a disordered nanoscopic system: the influence of the transition dipole orientation. Phys. Stat. Sol. (a) 205: 1258-1265.

[43] Froufe-Pérez LS, Carminati R (2007) Fluorescence decay rate statistics of a single molecule in a disordered cluster of nanoparticles. Phys. Rev. A 76: 013835.

[44] Rahmani A, Chaumet PC, de Fornel F (2001) Environment-induced modification of spontaneous emission: Single-molecule near-field probe. Phys. Rev. A 63: 023819.

[45] Zhang W, Cuib X, Martin OJF (2009) Local field enhancement of an infinite conical metal tip illuminated by a focused beam. J. Raman Spectrosc. 40: 1338-1342.

[46] Liaw JW, Chen JH, Chen CS, Kuo MK (2009) Purcell effect of nanoshell dimer on single molecule's fluorescence. Opt. Expr. 17: 13532-13540.

[47] Ferrie M, Pinna N, Ravaine S, Vallee RA (2011) Wavelength-dependent emission enhancement through the design of active plasmonic nanoantennas. Opt. Expr. 19: 17697-17712.

[48] Teperik TV, Degiron A (2011) Numerical analysis of an optical toroidal antenna coupled to a dipolar emitter. Phys. Rev. B. 83: 245408.

[49] Hohenester U, Trügler A (2011) MNPBEM-A MatLab toolbox for the simulation of plasmonic nanoparticles. Comp. Phys. Comm. 183: 370-381.

[50] Thomas M, Greffet JJ, Carminati R, Arias-Gonzalez JR (2004) Single-molecule spontaneous emission close to absorbing nanostructures. Appl. Phys. Lett. 85: 3863-3865.

[51] Rogobete L, Kaminski F, Agio M, Sandoghdar V (2007) Design of plasmonic nanoantennae for enhancing spontaneous emission. Opt. Lett. 32: 1623-1625.

[52] Mohammadi A, Sandoghdar V, Agio M (2008) Gold nanorods and nanospheroids for enhancing spontaneous emission. New J. Phys. 10: 105015.

[53] Mohammadi A, Kaminski F, Sandoghdar V, Agio M (2010) Fluorescence enhancement with the optical (Bi-) conical antenna. J. Phys. Chem. C 114: 7372-7377.

[54] Törmä P, Barnes WL (2015) Strong coupling between surface plasmon polaritons and emitters: a review. Rep. Prog. Phys. 78: 013901.

[55] Knight MW, King NS, Liu L, Everitt HO, Nordlander P, Halas NJ (2014) Aluminum for plasmonics. ACS Nano 8: 834-840.

[56] Kuzma A, Weis M, Flickyngerova S, Jakabovic J, Satka A, Dobrocka E, Chlpik J, Cirak J, Donoval M, Telek P, Uherek F, Donoval D (2012) Influence of surface oxidation on plasmon resonance in monolayer of gold and silver nanoparticles. Appl. Phys. 112: 103531.

[57] Della Sala F, D'Agostino S, editors (2013) Handbook of Molecular Plasmonics. Pan Stanford Publishing Pte Ltd.; DOI: 10.4032/9789814303217

[58] Moroz A (2010) Non-radiative decay of a dipole emitter close to a metallic nanoparticle: importance of higher-order multipole contributions. Opt. Comm. 283: 2277-2287.

[59] Gersten J, Nitzan A (1981) Spectroscopic properties of molecules interacting with small dielectric particles. J. Chem. Phys. 75: 1139-1152.

[60] Gersten J Theory of fluorophore-metallic surface interactions. In: Geddes CD, Lakowicz JR, editors. Topics in Fluorescence Spectroscopy, Vol. 8: Radiative Decay Engineering. Springer Science +Business Media, Inc; New York; 2005. p. 197-221. DOI: 10.1007/0-387-27617-3_6

[61] D'Agostino S, Pompa PP, Chiuri R, Phaneuf RJ, Britti DG, Rinaldi R, Cingolani R, Della Sala F (2009) Enhanced fluorescence by metal nanospheres on metal substrates. Opt. Lett. 34: 2381-2383.

[62] Vahala KJ (2003) Optical microcavities. Nature 424: 839-846.

[63] Goy P, Raimond JM, Cross MM, Haroche S (1983) Observation of cavity-enhanced single-atom spontaneous emission. Phys. Rev. Lett. 50: 1903-1906.

[64] Gabrielse G, Dehmelt H (1985) Observation of inhibited spontaneous emission. Phys. Rev. Lett. 55: 67-70.

[65] Bayer M, Reinecke TL, Weidner F, Larionov A, McDonald A, Forchel A (2001) Inhibition and enhancement of the spontaneous emission of quantum dots in structured microresonators. Phys. Rev. Lett. 86: 3168-3171.

[66] Martin OJF, Piller NB (1998) Electromagnetic scattering in polarizable backgrounds. Phys. Rev. E 58:3909-3915.

[67] Drexhage KH (1974) Interaction of light with monomolecular dye layers. Prog. Opt. 12: 163-232.

[68] Kleppner D (1981) Inhibited spontaneous emission. Phys. Rev. Lett. 47: 233-236.

[69] Lodahl P, van Driel AF, Nikolaev IS, Irman A, Overgaag K, Vanmaekelbergh D, Vos WL (2004) Controlling the dynamics of spontaneous emission from quantum dots by photonic crystals. Nature (London) 430: 654-657.

[70] Bian RX, Dunn RC, Xie XS (1995) Single molecule emission characteristics in near-field microscopy. Phys. Rev. Lett. 75: 4772-4775.

[71] Novotny L, Hecht B (2006) Principles of nano-optics. Cambridge University Press, New York.

[72] Alpeggiani F, D'Agostino S, Andreani LC (2012) Surface plasmons and strong light-matter coupling in metallic nanoshells. Phys. Rev. B 86: 035421.

[73] Yurkin MA, Hoekstra AG (2011) The discrete-dipole-approximation code ADDA: capabilities and known limitations. J. Quant. Spectrosc. Radiat. Transfer 112: 2234-2247.

[74] Code available at http://erbium.amolf.nl.

[75] Moroz A (2005) A recursive transfer-matrix solution for a dipole radiating inside and outside a stratified sphere. Ann. Phys. (NY) 315(2): 352-418.

[76] Moroz A. (2005) Spectroscopic properties of a two-level atom interacting with a complex spherical nanoshell. Chem. Phys. 317(1): 1-15.

[77] The F77 code CHEW, Copr. 06/2004 Alexander Moroz, can be downloaded at http://www.wave-scattering.com/codes.html.

[78] Palik ED (1985) Handbook of optical constants of solids. Academic.

[79] Xiao-Yong G, Hong-Liang F, Jiao-Min M, and ZengYuan Z (2010) Spectroscopic ellipsometric study of the optical properties of Ag_2O film prepared by direct-current magnetron reactive sputtering. Chin. Phys. 19: 090701.

[80] D'Agostino S, Della Sala F (2010) Active Role of Oxide Layers on the Polarization of Plasmonic Nanostructures. ACS Nano 4: 4117-4125.